Chapter 7

Light Transmission via Subwavelength Apertures in Metallic Thin Films

V. A. G. Rivera, F. A. Ferri, O. B. Silva, F. W. A. Sobreira and E. Marega Jr.

Additional information is available at the end of the chapter

http://dx.doi.org/10.5772/50807

1. Introduction

The optical properties of subwavelength apertures in metallic films have been the focus of much research activity around the world since the extraordinary optical transmission (EOT) phenomenon was reported over a decade ago (Ebbesen et al., 1998).

EOT is an optical phenomenon in which a structure containing subwavelength apertures in an opaque screen transmits more light than might naively be expected on the basis of either ray optics or even knowledge of the transmission through individual apertures. The phenomenon was discovered serendipitously for two-dimensional (2D) periodic arrays of subwavelength holes in metals (Garcia-Vidal et al., 2010). Surprisingly, such arrays may, for certain wavelengths, exhibit transmission efficiencies normalized to the total area of the holes that exceed unity. In other words, for these wavelengths a periodic array of subwavelength holes transmits more light than a large macroscopic hole with the same area as the sum of all the small holes. The surprise is compounded by the fact that a single subwavelength aperture generally transmits light with an efficiency that is substantially below unity.

This remarkable transmission enhancement has potential applications in photolithography, near-field microscopy, and photonic devices (Lal et al., 2007). Although the detailed picture of the transmission enhancement is still being investigated, the excitation of surface plasmon-polaritons (SPPs) is proposed to be involved in the process (Weiner, 2009). Ever since the first experimental report on EOT through subwavelength apertures, considerable theoretical effort has been devoted to interpreting the essential physics of the process in slit arrays (Porto et al., 1999; Takahura, 2001; Xie et al., 2005). Experimental studies subsequent to the initial report were also performed, which demonstrated a number of surprising features. For instance, spectral transmission measurements (Lezec et al., 2004) revealed that suppression, as well as enhancement, was a characteristic property of slit arrays. Additionally, interferometric studies (Gay et al., 2006a, 2006b; Kalkum et al., 2007) showed

that the contribution of transient diffracted surface modes is as important as the SPP guided mode in the immediate vicinity of the subwavelength object. A more recent investigation (Pacifici et al., 2008) with the aim to confront the question of how transmission minima and maxima depend on array periodicity showed a minimum in transmission at slit separations equal to the wavelength of the SPP mode, and maxima occurring approximately at half-integer multiples.

These previous studies focused attention on the properties of arrays fabricated in metallic films. It was already shown that a single slit is an interesting structure, since it combines the compactness of a single defect with the directionality of an array launcher. The extended dimension of the long axis imposes directionality on the transmitted light beam, the divergence of which can easily be controlled (Laluet et al., 2008). In a very recent investigation dealing with single subwavelength slits, it was possible to observe that the slit transmission is notably affected by the film thickness, and increases linearly with increasing slit width for a fixed film thickness (Ferri et al., 2011).

In this chapter, we selected some fundamental subjects of high and general interest involved in the phenomenon of light transmission via subwavelength apertures in metallic thin films. The manuscript will cover issues on both theory and experiment, such as (1) fabrication and measurement setup characteristics, (2) different materials and metallic structures, and (3) phenomena from the metallic film/dielectric interface. In addition, numerical simulations were performed in order to investigate the optical transmission through subwavelength apertures.

The paper is organized as follows. In Section 2, we comment on the classical theories of diffraction by subwavelength apertures. In Section 3, a rapid discussion about preceding experiments and interpretations are presented. In Section 4, we give a simple introduction to the plasmon-polariton. In Section 5, some characteristics of focused-ion beam (FIB) nanofabrication are presented. In this manner, the topics covered by the above mentioned sections are basically a compilation of information found in literature. In Section 6, we in fact demonstrate some applications made by our research group investigating the (1) influence of the metallic film thickness, as well as the (2) use of multilayered metallic thin films on the optical transmission through subwavelength slits. A short summary is provided in Section 7.

2. Diffraction by subwavelength apertures

The wave nature of light implies modifications in the transmission through apertures like the phenomenon of diffraction. This common process, that even in simple geometries is very complex, have been extensively studied and many different models and approximations were developed based on the classical theory of diffraction (Jackson, 1999; Bouwkamp, 1954). Probably the simplest geometry, and maybe for this reason one that received the most attention, is that of a circular aperture with radius r in an infinitely thin and perfect conducting screen (Fig. 1).

If the radius r of the aperture is some orders of magnitude larger than the wavelength λ_0 of the impinging radiation, i.e., $r \gg \lambda_0$, the problem can be treated with the Huygens-Fresnel principle and its mathematical formulation can be given as a good approaching by the

Kirchhoff scalar theory of light diffraction (Jackson, 1999). This theory is based on a scalar wave theory, and, thus, it does not take into account effects due to the polarization of light. In the case of normal incidence of light through a circular aperture, it is easy to show that the transmitted intensity (dI) per unit solid angle (dΩ) in the far-field region, also known as Fraunhofer diffraction limit, is given by $I(\theta) \cong I_0 \left(k^2 r^2 / 4\pi\right) \left|2J_1(krsin\theta) / krsin\theta\right|^2$, where the incident intensity I_0 is equally distributed on the aperture area πr^2. The wavenumber of the incident light is $k=2\pi/\lambda_0$, θ is the angle between the normal to the aperture and the direction of the emitted radiation, and $J_1(krsin\theta)$ is the Bessel function of the first kind. The pattern described by this formula is the well known Airy pattern, composed by a central bright spot surrounded by concentric bright rings of decreasing intensity, caused by the interference of light rays originated inside the aperture (see Fig. 1). The ratio of the total transmitted intensity to I_0, given by $T = \int I(\theta) d\Omega / I_0$, is called the transmission coeficient. For large apertures, with $r \gg \lambda_0$, in which case the treatment is outlined here is valid, $T \approx 1$.

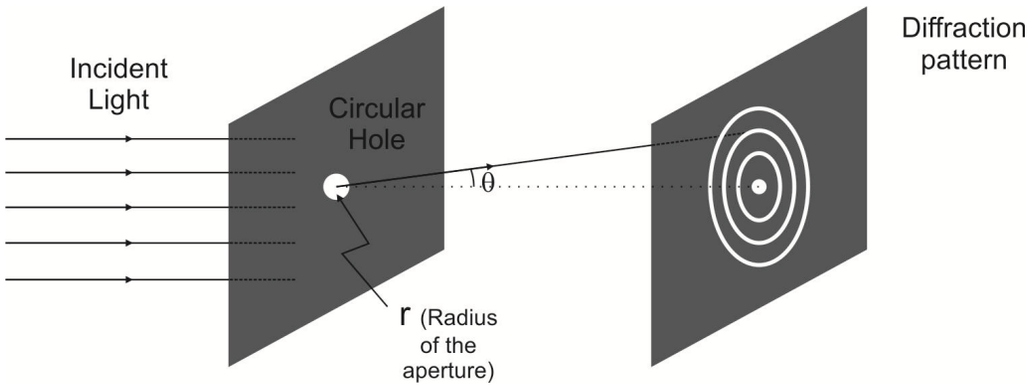

Figure 1. Transmission of light through a circular aperture or radius r in an infinitely thin opaque screen

It has been proposed (Weiner, 2009) that the existence of surface waves such as SPPs are involved in the transmission process. For this reason, the regime of subwavelength apertures $r \ll \lambda_0$ is much more interesting, because near-field effects are expected to contribute dominantly in the transmission process. The problem arising here is that even in an approximate analysis of a perfectly conducting screen in the limit of zero width, we must use a vector description via Maxwell's equations. In Kirchhoff's method, the basic assumption is that the electromagnetic field in the aperture is the same as if the opaque screen is not present, a case which does not fulfil the boundary condition of zero tangential electric filed on the screen. For large holes, in which $r \gg \lambda_0$, this basic failure is less severe, because the diffracted fields are small when compared to the directly transmitted ones. Nevertheless, for subwavelength apertures this approximation is inadequate even in a first order treatment of the problem.

Assuming that the incident light intensity I_0 is constant over the area of the aperture, Bethe and Bouwkamp arrived at an exact analytical solution for light transmission through a sub-wavelength circular hole in an ideal perfectly conducting and infinitely thin screen (Bethe, 1944; Bouwkamp, 1950a; Bouwkamp, 1950b). For normal incidence, the aperture can be described as a magnetic dipole located in the plane of the hole. The transmission coefficient for an incident plane wave is then given by (Maier, 2007)

$$T = \frac{64}{27\pi^2}(kr)^4 \propto \left(\frac{r}{\lambda_0}\right)^4 \quad (1)$$

There is a weak total transmission for a subwavelength aperture due to the scaling with $(r/\lambda_0)^4$, smaller by an amount of $(r/\lambda_0)^2$ compared to Kirchhoff's scalar theory. This scaling of $T \propto \lambda_0^{-4}$ is in agreement with the theory of light scattering by small objects due to Rayleigh. The case described in Eq. (1) is that of normal light incidence with both transverse electric (TE) and transverse magnetic (TM) polarization. This is not the case when radiation is incident in the screen at another angle, in this case an additional electric dipole in the normal direction is needed to describe the different behaviour of the process. More radiation is transmitted for TM than for TE polarization in this case (Bethe, 1944).

There are two major approximations in the Bethe-Bouwkamp theory of light transmission through a circular aperture in a screen. The screen is said to be made of an ideal perfectly conducting screen, and so perfectly opaque to the transmission of radiation, and its thickness is taken to be infinitely small. One of these assumptions could be omitted by taking numerical simulations for the problem of screens with finite thickness (Maier, 2007). However, when discussing the transmission properties through real apertures, i.e., in real metals, the finite conductivity, and so the transmission, should be taken into account. The thin films used in optical experiments cannot be taken as perfectly opaque screens, and we could not employ the Bethe-Bouwkamp theory. On the other hand, if the film thickness is higher than some skin depths, that is, if we are dealing with a "thick" film, it could be taken as an opaque screen. It has been shown that for apertures fulfilling these conditions, localized surface plasmons have a significant influence in the transmission process (Degiron et al., 2004).

3. Early experiments and implications

In the paper published by Ebbesen et al., it was affirmed the measurement of "transmission efficiency...orders of magnitude greater than predicted by standard aperture theory". A typical result obtained in the original experiments is shown in the right panel of Fig. 2. The figure shows the transmitted power as a function of the incident light wavelength λ through a circular aperture of radius r. The transmission intensity is normalized to the cross-sectional area of the hole $A=\pi r^2$. Using the experimental parameters of the caption of Fig. 2, the efficiency predicted by Bethe theory, given by Eq. (1), is 0.34%, while the results obtained by Ebbesen et al. reported peak efficiencies of a factor more than two. In this case, the enhancement of light transmission over that expected by Bethe theory is about 600 times. In a following paper (Ghaemi et al., 1998) the same group reported peak transmission efficiencies "that are about 1000 times higher than that expected for subwavelength holes". To obtain an EOT it is plausible to say that would be necessary at least a three-order of magnitude increase over the predictions of Bethe formula.

It was proposed in these early reports that transmission enhancements were caused by a new phenomenon not taken into account in electromagnetic (E-M) vector field Bethe theory nor in the scalar diffraction Kirchhoff model: the resonant excitation of surface plasmons

(SP) waves supported by the periodic array structure in the metal film. The physics of SP waves shall be discussed in the next Section. About a year later Treacy suggested (Treacy, 1999) "dynamic diffraction" as another model to investigate the problem of light transmission through a periodic array of holes or slits. It was pointed out that the oscillation at frequency ω of the optical field would induce currents within the skin depth of the metal. The periodic structuring of holes in the metal gives rise to Bloch modes of the E-M field induced in the metal within the skin depth and consistent with its periodicity. There will be an oscillating current associated to each of these Bloch modes. Then, Treacy invoked "interband scattering" as a way to distribute these energy among these Bloch modes and from there to the propagating modes and surface waves at the aperture exit. It was not exactly clarified how does this redistribution occurs, but Treacy suspected that the success of "dynamic diffraction" for interpreting X-ray scattering in crystals might be useful for the understanding of light transmission through these new structures as well.

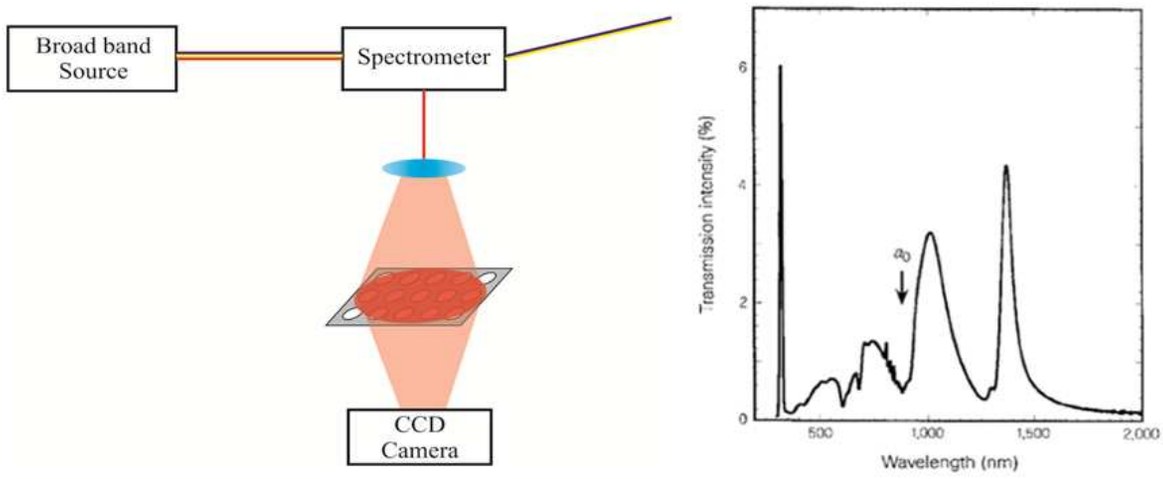

Figure 2. Left panel: schematic of the original spectral transmission experiments. A broadband, incoherent light source is spectrally filtered by a scanning spectrophotometer and focused onto an array of subwavelength structures (holes or slits). A charge-coupled device (CCD) camera records the transmission intensity through the structure as a function of wavelength of the input light (adapted from Weiner, 2009). Right panel: transmission spectrum from an array of holes in an Ag metal film evaporated onto a transparent substrate as reported by Ebbesen et al. Array periodicity: 900 nm, hole diameter: 150 nm, metal film thickness: 200 nm. The point indicated a_0 marks the array periodicity

A much more complete presentation of dynamic diffraction was published two years later by Treacy (Treacy, 2002). In this work it was clarified the relation between this approach and earlier interpretations of transmission in terms of "resonant" excitation of SP waves. This pioneering paper pointed out the way forward by emphasizing critical factors in the proper analysis of the problem. The most important thing to observe is that Bloch modes are determined by the E-M field present on and below the metal surface where are placed the periodic structures. These modes obey the periodic boundary conditions of the structure independently of the wavelength of the incident light. The simplest case is that of a one dimensional (1D) structure, with arrays and/or grooves placed periodically. In this case the modes are parallel to the surface in the metal and in the dielectric media, and evanescently

vanishing in the normal direction. In parallel to this there are propagating modes. These propagating modes are responsible for the transmission of light through the structures. The transmission of the E-M filed is defined by both, propagating and evanescent fields, as a result of linear combinations of Bloch modes.

4. Plasmon-polaritons

It is important to stress here that metals play a more important role in plasmonics than dielectric media (Huang et al., 2007). In a metal, the optical as well as the electric properties are very different from dielectrics because of the existence of huge free electrons. These electrons have a fast response to varying fields leading to a different response than that in a dielectric media.

In the Drude model for free electrons, the dielectric constant is given by

$$\varepsilon_m = 1 - \frac{\omega_P{}^2}{\omega(\omega + i\gamma)} \tag{2}$$

The constant ω_P is called the bulk plasma frequency and is a constant that depends on the metal. The constant γ is associated to the scattering of electrons in the Drude model. In "good" metals, where the scattering process is reduced we can neglect the damping ($\gamma = 0$). For high frequencies the dielectric constant is positive and there are modes whose dispersion relation is given by $\omega^2 = \omega_P{}^2 + c^2k^2$. In this expression, c is the light velocity in vacuum. These modes are known as bulk plasmon-polaritons (BPPs) and are a result of the coupling between light and the free electrons in metals. For light at low frequencies, which is the case of visible light for metals, then $\omega < \omega_P$, and light propagation is forbidden by the negative permittivity.

For the case of a metal, whose real part of permittivity is negative, light incident normally to the surface gives rise to evanescent modes. But even in metals, there are propagating modes in the surface of the metal, provided that the surface of the metal is interfaced with a dielectric (or vacuum). These modes are the so-called SPP waves mentioned before. A typical geometry for this kind of problem is a metal and a dielectric separated by an infinite plane surface, as shown in the left panel of Fig. 3. This surface wave is based on the coupling between the surface free charges along the metal and light. In this case, the dispersion relation is given by (Zayats et al., 2005):

$$k_{SPP} = \frac{\omega}{c}\sqrt{\frac{\varepsilon_m \varepsilon_d}{\varepsilon_m + \varepsilon_d}} \tag{3}$$

Here, ε_d is the permittivity of dielectric. The condition for the propagation of the SPP is that k_{SPP} is real. As the permittivity of metal is negative it is necessary that $\varepsilon_m + \varepsilon_d < 0$, in this case $\omega < \omega_{SP} \equiv \omega_P/\sqrt{1+\varepsilon_d}$, where ω_{SP} is the surface plasmon frequency. The dispersion relation for the SPPs and BPPs are plotted schematically in the right panel of Fig. 3. The left panel of Fig. 3 shows the mechanism of how the surface plasmon propagates along the metal/dielectric surface.

Some features of the SPP propagation along these flat interfaces between a metal and a dielectric, as summarized by Huang et al., are addressed in the following.

It was discussed that SPP modes are the result of a coupling between the free electrons in the metal side and light (E-M field). The modes given by the dispersion relation in Eq. (3) are called TM modes. These are the only allowed modes, in the case of an interface between two non-magnetic media, and are characterized by a magnetic field normal to the propagation direction (in the left panel of Fig. 3 it is normal to the plane of the paper) and an electric filed that has components parallel ($E_{//}$) and normal ($E_{\perp}$) to the direction of propagation (the plane of the paper in Fig. 3). The ratio of the normal and parallel components of electric field inside the dielectric $(E_{\perp}/E_{//})_d = \sqrt{\varepsilon_m/\varepsilon_d}$ and inside the metal $(E_{\perp}/E_{//})_m = -\sqrt{\varepsilon_d/\varepsilon_m}$ shows that, inside the metal, as the electric field is almost completely concentrated in the direction of propagation, the free electrons present a movement of back and forth in the direction of propagation. These are the electron density waves shown in Fig. 3.

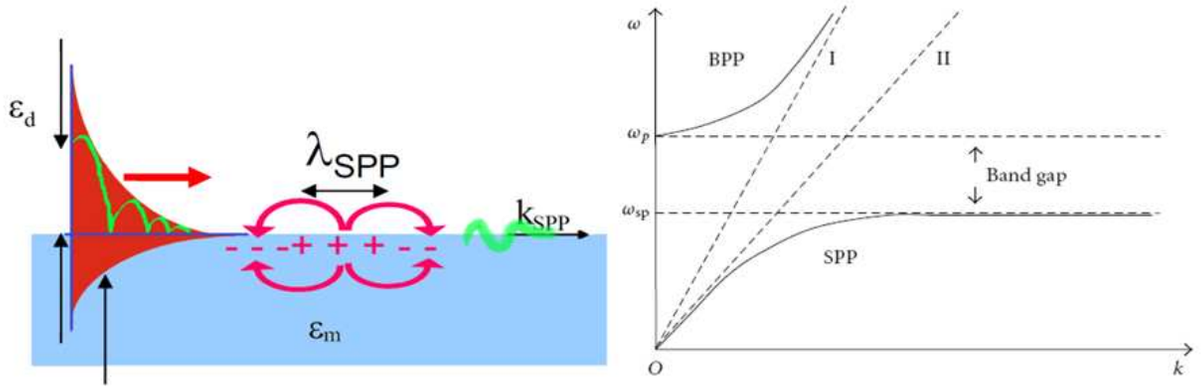

Figure 3. Plasmon-polariton modes associated with the metals. Left panel: SPP mode in a schematic view of infinite metal/dielectric interface. Right panel: dispersion relation of BPP and SPP modes. The dashed lines I and II denote the light dispersion $\omega = ck$ and $\omega = ck/\sqrt{\varepsilon_d}$, respectively. The frequency range between ω_{SP} and ω_P corresponds to a gap where the electromagnetic wave cannot propagate via either bulk or surface modes (Huang et al., 2007)

The SPP modes propagate along the interface between media with a larger propagation constant ($k_{SPP} > k_0\sqrt{\varepsilon_d}$), so the wavelength and propagation velocity are smaller than in vacuum. Taking into account that the metal permittivity still has a negative part, that is responsible for losses, the propagation of SPP is reduced to a finite value given by the propagation length $L_{SPP} \approx \varepsilon_m'^2/k_0\varepsilon_m''\varepsilon_d^{3/2}$, where ε_m' and ε_m'' are the real and imaginary parts of metal permittivity, respectively. In visible and near-infrared region, L_{SPP} can take values of several micrometers, as can be seen in Fig. 4, that shows the real and imaginary parts of permittivity for Au and Ag [Fig. 4(a)], and the propagation length for each of these media with an interface with air [Fig. 4(b)].

The confinement of SPP modes along the surface is characterized by its evanescent behaviour in either side of the interface, which happens because of the larger propagation constant. On the dielectric side there is a higher penetration of the E-M field, given by the

decaying length $\delta_d \approx \sqrt{|\varepsilon_m'|}/k_0\varepsilon_d$. On the metal side, where the decaying length is $\delta_m \approx 1/k_0\sqrt{|\varepsilon_m'|}$, there is a higher confinement than in the dielectric side. The relation between these lengths δ_d/δ_m is about some tens. This is what is desired in practice. Moreover, there is a strong enhancement of the fields near the interface of the media.

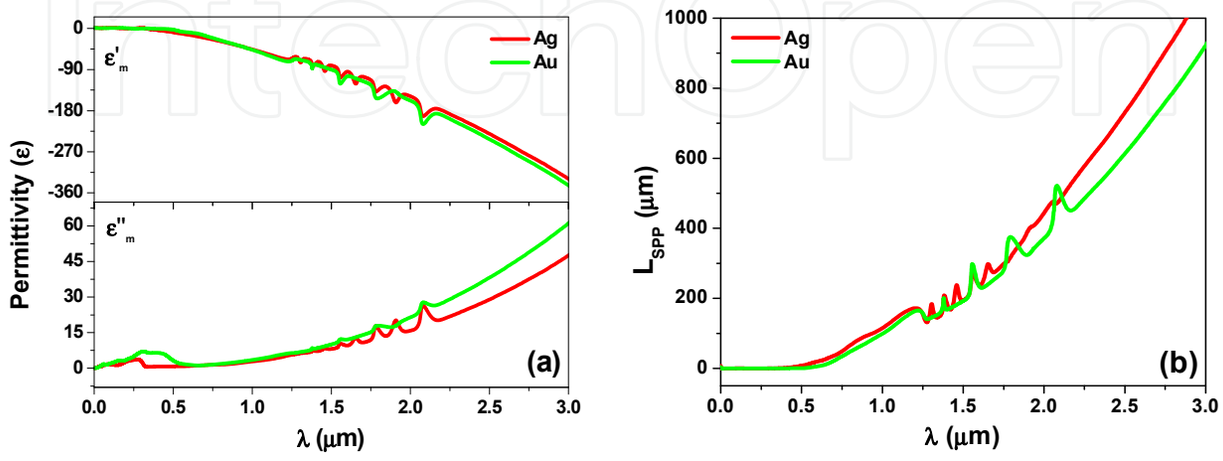

Figure 4. (a) Real ε_m' and imaginary ε_m'' parts of permittivity for Au and Ag as obtained using data from Palik, and the corresponding (b) Propagation length L_{SPP} as a function of the wavelength. In this case it is considered an interface between metal and air, whose permittivity is taken to be unity

SPP modes cannot be excited directly by the incident light because of its larger propagation constant. Special techniques have been used (Zayats et al., 2005) to compensate the phase mismatch as well as the difference in the wavevectors. Some of these techniques employ, for example, prism coupling by attenuated total reflection and diffraction gratings. It is also possible to couple plasmons by near-field excitation with a near-field optical microscope. An efficient mode to excite SPP is a subwavelength hole or slit (Zayats et al., 2005; Yin et al., 2004; Lalanne et al., 2005), where the diffraction components can ensure momentum conservation. Because of its localized feature, a direct observation of SPP is very difficult. Some methods, like the observation by using near-field microscopy (Hecht et al., 1996) can be used for this purpose. It is also possible to map SPP modes by recording the scattered light from a metal surface (Bouhelier et al., 2001) prepared with structured nanoscale corrugations. Another method, called fluorescence imaging (Ditlbacher et al., 2002a), has been proposed and consists in a metal surface covered with fluorescent molecules which emit radiation with intensity proportional to the electric field. This method was successfully used to observe interference, beam splitting and reflection of SPP modes (Ditlbacher et al., 2002b).

It is also important to note that even in more complex cases of metal/dielectric interfaces, SPP modes can exist with some parallel characteristics. A good example is that of a thin metal film where the thickness is of the same order of the skin depth. In this case, the SPP modes excited in each of its surfaces couple together and give rise to the so-called long-range SPP modes (Sarid, 1981). There is also a current research interest in particle plasmon-

polariton modes that are excited in particles with have dimensions much smaller than the E-M wavelength. A detailed discussion on this topic can be found in (Hutter et al., 2004).

5. Focused-ion beam nanofabrication

Plasmonic structures can be obtained by many standard techniques, some of them are: optical lithography, electron-beam lithography, focused-ion beam (FIB) lithography, atomic layer deposition, soft lithography and template stripping (Lindquist et al., 2012). Taking into account that in the present work FIB lithography was extensively used, we will briefly discuss here only this fabrication technique. A comprehensive discussion of the other mentioned techniques (as well as FIB lithography) is very well presented in the work by Lindquist et al.

FIB lithography has been extensively used for direct fabrication of metallic nanostructures, by making patterns on substrates (Melngailis, 1987; Orloff et al., 1993; Langford et al., 2007). It can also be used for the deposition of various metals by using ion-beam induced deposition (Tao et al., 1990), for doping semiconductors (Melngailis, 1987; Moberlychan et al. 2007), and for preparing transmission electron microscope (TEM) samples (Reyntjens et al., 2001; Mayer, 2007). These methods proved to be very useful to make tests of device designs and geometries, fix masks or electrical traces, or to produce high-resolution ion-beam images, and have been an essential tool for the development of the field of plasmonics.

FIBs impinging on a surface offer a very different form of nanopatterning compared with other conventional methods that use resist, exposure and development. In general, the accelerating potential of the ions is of tens of kilovolts, the current beams range from many orders of magnitude, from picoamps to several nanoamps. Depending on the column optics, ion source and beam current, the beam spot sizes can range from ~ 5 nm up to a micrometer. Numerous ion species can be used in the setup, such as Al, Au, B, Be, Cu, Ga, Ge, Fe, In, Li, P, Pb and Si, the most commonly used being the semiconductor dopants (Melngailis, 1987; Orloff et al., 1993). In particular, Ga is widely used due to its low melting temperature (30 °C), low volatility and low vapour pressure (Volkert et al., 2007).

The FIB system is based on a liquid-metal ion source which is used to produce a smaller and brighter ion beam (Volkert et al., 2007). A metal source is heated up, such that it flows down and wets a sharp tungsten needle. An extraction voltage applied between the metal source and an extraction aperture forces the liquid metal to be pulled into an extremely sharp "Taylor–Gilbert" cone (Volkert et al., 2007; Forbes et al., 1996). The balance between the electrostatic force produced by the extraction voltage and the surface tension forces in the liquid (Orloff et al., 1993), the liquid source can have a tip size on the order of several nanometers (Melngailis, 1987). Then, the ions are extracted from the tip of this cone by field emission. As opposed to e-beam imaging systems, the "lenses" used in FIB are electrostatic and not magnetic, this happens because the Lorentz force in heavy ions, as those used, is much smaller than in electrons with the same kinetic energy (Volkert et al., 2007). Some other similarities and differences in these two kind of systems is presented in Fig. 5(a). To make the patterns a fast beam blanker is used. In commercial systems many patterns can be drawn by using pre-fabricated CAD proprietary files or using options within the control

software. The final size and the resolution of the focused beam can, in general, be affected by chromatic aberration, i.e., the energy dispersion of ions in the beam, but with a good approximation it can be regarded as a Gaussian profile. The minimum beam size is on the order of ~ 5 nm. A schematic view of the ion source is shown in Fig. 5(b).

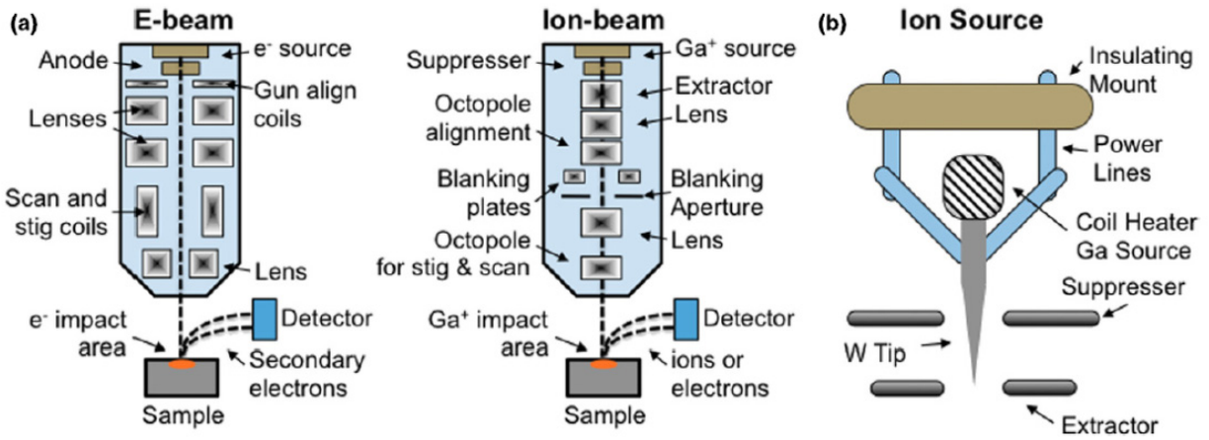

Figure 5. (a) Schematic view showing the similarities and differences between typical e-beam and FIB systems. (b) Scheme of the gallium liquid-metal source (Lindquist et al., 2012)

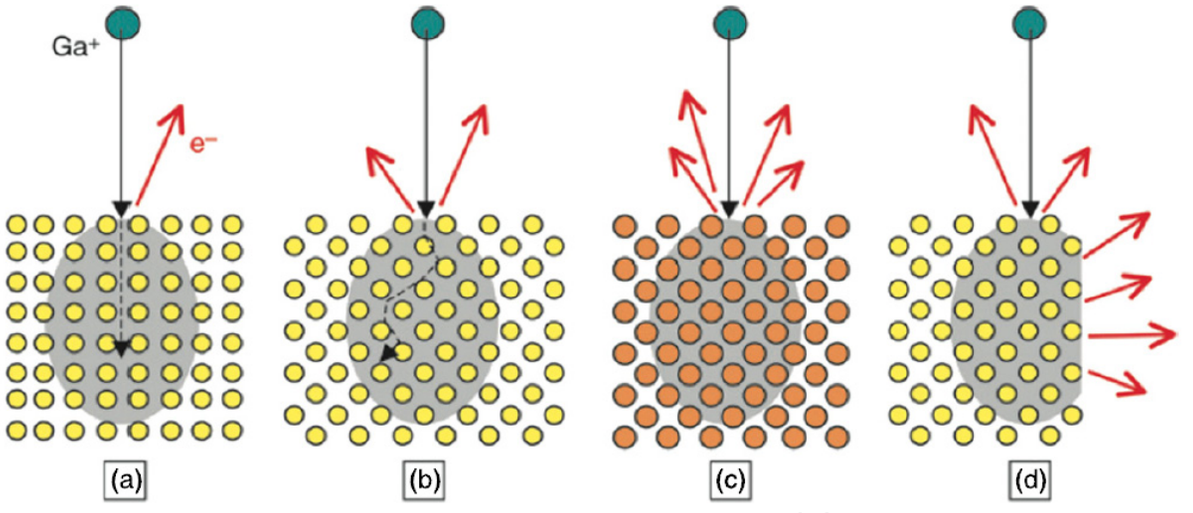

Figure 6. The crystal orientation of a sample can affect the FIB sputtering rates, shown in (a) and (b). (c) The sputtering rate is also affected by the mass of the atoms (orange atoms are more massive) and (d) by the local geometry of the sample (Lindquist et al., 2012). Original figure from Volkert et al.

In the process of milling a substrate by using FIB, many effects can be produced, with approximately one to five atoms removed per incident ion depending on the ion energy or substrate. It is even possible to displace atoms from their equilibrium positions, to induce chemical reactions and use the emerging electrons for imaging. The Gaussian profile of the beam is not the only factor that the shape of the milled groove depends (Melngailis, 1987). Redeposition and self-focusing effects can lead to large geometric differences depending on

whether the patterns designed were done in single of multiple steps, even with the same overall dose. Also, milling a trench with large total ion doses deviates from the Gaussian profile, giving an unexpectedly deep, V-shaped groove (Melngailis, 1987). The FIB milling process depends on many aspects such as the material to be patterned, ion-beam incident angle, redeposition of sputtered materials and even the crystal orientation, as outlined in Fig. 6. Grain orientation-dependent FIB sputtering can also lead to severe surface roughness on polycrystalline samples, however, care can be taken to produce well-defined structures (Lindquist et al., 2012).

FIB can also be used for the deposition of various metals (such as W, Pt, C and Au) via site-specific chemical vapour deposition (CVD), this can be done by using a gas injection system (GIS) (Volkert et al., 2007). A high-efficiency deposition can be achieved, with about 1 μm per minute accumulation rates, by adjusting the gas precursor flow rates and the ion-beam current density. The reaction of the ion beams with the precursor materials offers the ability to weld micromanipulators to specific parts of a substrate in situ. With subsequent FIB milling and thinning, those parts are cut free, and are often mounted to a TEM imaging grid (Mayer, 2007). A deficiency of this kind of system is that metals deposited via FIB have a high contamination by carbon. It can also be used other GIS systems, instead of depositing metals, to enhance the inherent FIB milling etch rate.

FIB instruments offer many significant advantages, like a direct write, maskless, high-resolution nanofabrication with the ability to sputter, image, analyse and deposit. It is possible to design 2D and 3D patterns (Langford et al., 2007). However, it has some limitations as a patterning tool, particularly for metals. FIB milling is a serial lithography technique, such as e-beam lithography, patterning only one spot or device at a time, unlike optical lithography that patterns the whole wafer with one short exposure. Large area patterning is not feasible. For high-resolution (< 100 nm) features, FIB milling can also be slow since very low currents (~ pA) must be used. Along with FIB-induced sample damage (Mayer, 2007), Ga ions are implanted at atomic fractions of 1–50% near the sample surface (Volkert et al., 2007). The plasmonic properties of the patterned metal films can be degraded is this process. For high surface roughness of metals the SPP propagation length can be strongly reduced (Lindquist et al., 2012). As such, the advantages and disadvantages of FIB milling need to be taken into account when fabricating new optical or electronic devices. When combined with a template stripping technique, many of these roughness and contamination issues are minimized, since FIB is then used to only pattern a reusable template, leaving the resulting metal films smooth and contamination-free (Lindquist et al., 2012).

6. Applications: Optical transmission through subwavelength single slits

6.1. Influence of metallic film thickness

6.1.1. Motivation

By focusing attention on the properties of arrays fabricated in metallic films with fixed thickness, some previous studies mentioned in Section 1 apparently missed the important

role played by the film thickness. For example, in the designing of surface-plasmon-based sensors, a proper choice of the thickness of the metallic film for the optimization of the device sensitivity is very important (Fontana, 2006). There are only a few theoretical (Xie et al., 2005; Fontana, 2006; Janssen et al., 2006) and experimental (Shou et al., 2005; Kim et al., 2006; Pang et al., 2007) investigations taking into account the influence of film thickness on the considered process. Therefore, the present studies are motivated by the necessity to understand the physics of this phenomenon and to develop optimum designs practices for subwavelength structure fabrication. We present here a systematic study of the optical transmission through subwavelength slits fabricated in Ag and Au film samples possessing different thicknesses. The influence of slit width was also considered. The present work deals with single slits. The extended dimension of the long axis imposes directionality on the transmitted light beam, the divergence of which can easily be controlled (Laluet et al., 2008). A slit is thus an interesting structure since it combines the compactness of a single defect with the directionality of an array launcher. Moreover, in order to remove measurement ambiguities existing in setups employing an incoherent and broadband light source dispersed through a scanning spectrophotometer, as shown in the left panel of Fig. 2, we have measured the transmission intensity through the slits using coherent and monochromatic spectral sources (Pacifici et al., 2008; Ferri et al., 2011).

6.1.2. Experimental considerations

A series of Ag films with thicknesses of 120, 160, 200, 270, and 330 nm and a set of Au samples with thicknesses of 120, 180, 260, 360, and 450 nm, as measured by a Talystep profilometer, were thermally evaporated onto BK7 glass substrates. Slits with widths in the range of approximately 70–150 nm in the Ag films, and 120–270 nm in the Au films, were milled with an FEI focused ion beam QUANTA 3D 200i (Ga^+ ions, 30 keV). In order to verify the depth of the slits, the gallium ions' source was calibrated using atomic force microscopy. For example, the right panel of Fig. 7 shows a scanning electron micrograph of a slit with 150 nm of width fabricated in the 200 nm thick Ag film.

We have undertaken a series of high-resolution measurements of the optical transmission through the slits. The transmission measurement setup consists of 488.0 nm (for Ag) and 632.8 nm (for Au) wavelength light beams from Ar ion and HeNe lasers, respectively, with a power of about 1 μW, aligned to the optical axis of a microscope. The beam is focused at normal incidence onto the sample surface by a 20× microscope objective (with an NA of 0.4) in TM polarization (magnetic field component parallel to the long axis of the slits). Light intensity transmitted through each slit is then gathered by an optical fibre and detected with a CCD array detector. It was used on a multimode fibre with an NA of 0.22 and a core diameter of 200 μm. Light intensity is obtained by integrating the signal over the entire region of interest in the CCD image and subtracting the background originating from electronic noise. The transmitted intensity of every slit was recorded in the far-field by the CCD as the sample was stepped using an x-y translation stage. The left panel of Fig. 7 shows the schematic of the measurement setup.

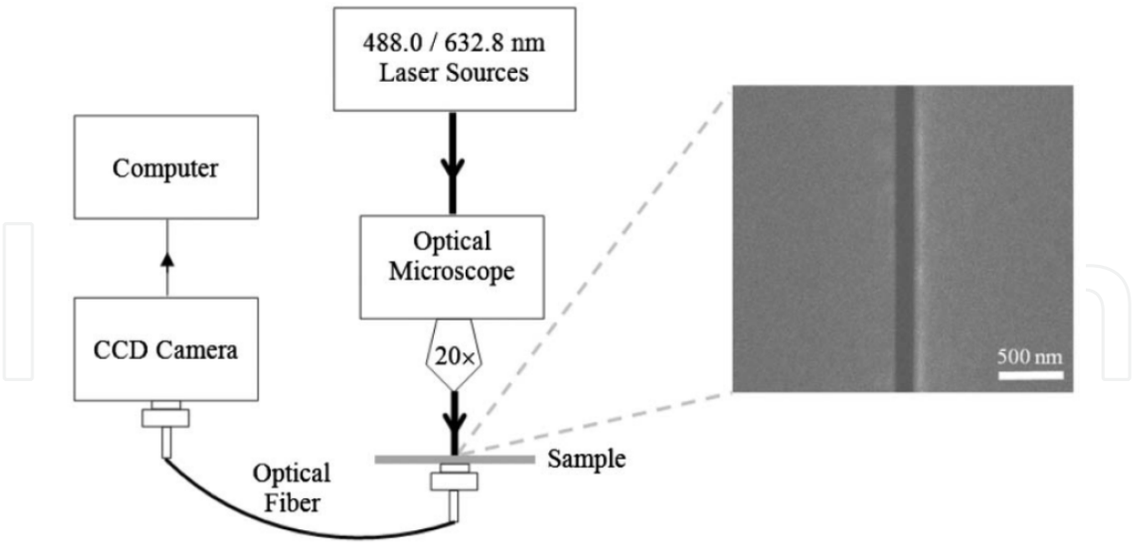

Figure 7. Left panel shows a schematic of the optical transmission experiment. 488.0 nm (for Ag) and 632.8nm (for Au) Ar ion and HeNe laser light sources, respectively, are normally focused onto the sample surface by a 20× microscope objective lens. A CCD camera records the transmission intensity through the slits as the sample surface was stepped. Right panel shows a scanning electron micrograph (taken with 40000× magnification) of a typical structure. The considered slit has approximately 150 nm of width and was focused-ion-beam milled through a 200 nm thick Ag layer. In the experiments, the thicknesses of the Ag and Au films were varied in the range of 100–450 nm. The width is varied from 70 to 270 nm (Ferri et al., 2011)

6.1.3. Results and discussion

Fig. 8 shows the physical picture adopted in this work to investigate the light transmission through the subwavelength slits. The essential elements of the model, which describes a plasmonic damped wave with amplitude decreasing as the inverse of the film thickness (Gay et al., 2006b), are represented in the sketch of Fig. 8. Basically, an incident monochromatic light beam with wave vector k_0 in air is linearly polarized perpendicular to the slit of subwavelength width w, milled in a metallic film with thickness t, and deposited on a dielectric substrate (BK7 glass).

The far-field intensity enhancement for the single slits involves multiple coupling processes (see Fig. 8). Initially, the incident laser light generates SPs on the metal film. Because of vertical plasmon coupling, which depends on the film depth (t), surface charges are induced on the top metal film and simultaneously a strong electric field is generated inside the slit. Subsequently, an SPP mode (Maier, 2007), i.e., an electromagnetic excitation propagating at the interface between the dielectric and the metallic conductor, evanescently confined in the perpendicular direction, is generated on the metal film/BK7 interface. The SPP evanescent mode travels along the interface toward the slit, where it reconverts to a propagating wave and interferes with the travelling field directly transmitted through the slit. Additionally, penetration of the incident field inside the film enables the excitation of localized SP resonances (Maier, 2007) on the rim of the aperture, which contribute to the superposed

output field. In this way, induced dipole moments at each rim form an "antenna coupling", which radiatively generate strong field enhancement (top and bottom). Then, the intensity of the resulting field can be written as

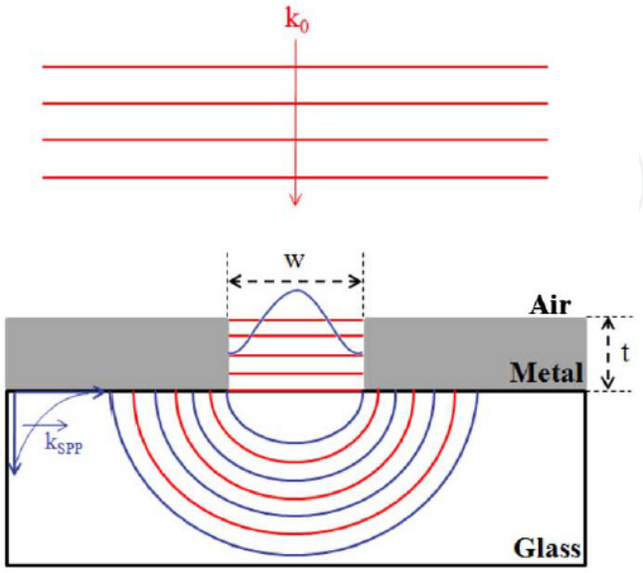

Figure 8. Illustration of the adopted model. A single frequency incoming plane wave with wave vector k_0 in air is linearly polarized perpendicular to a slit of subwavelength width w, milled in a metallic film with thickness t deposited on a BK7 glass substrate. Here, k_{SPP} is the wavevector of the SPP mode. (Ferri et al., 2011)

$$E \approx \frac{E_0}{\pi}\frac{w}{t}\cos\left(k_{SPP}t + \frac{\pi}{2}\right) \tag{4}$$

where $k_{SPP} = 2\pi/\lambda_{SPP}$, $\lambda_{SPP} = 2\pi/\mathrm{Re}[\beta]$, $\beta = k_0 n_{SPP}$, $n_{SPP} = \left(\varepsilon_{metal}\varepsilon_{glass}/\varepsilon_{metal} + \varepsilon_{glass}\right)^{1/2}$, and $k_0 = 2\pi/\lambda_0$ (Gay et al., 2006b; Pacifici et al., 2008; Maier, 2007). Here, E_0 represents the electrical field of the incoming plane wave, where λ_0 is its wavelength. Also, k_{SPP} and λ_{SPP} are the wavevector and wavelength of the SPP, β is the propagation constant of the superposed travelling wave, and n_{SPP} is the effective index of the SPP, which is for the interface between the metal and dielectric. In addition, ε_{metal} and ε_{glass} are the dielectric permittivities of metal and glass, respectively, and are functions of the excitation wavelength. In this sense, ε_{Ag} = - 7.89 + 0.74i and ε_{glass} = 2.31 are the tabulated dielectric constants of Ag and BK7 glass in the wavelength of 488.0 nm. In the same way, ε_{Au} = - 9.49 + 1.23i and ε_{glass} = 2.29 are the corresponding dielectric constants of Au and BK7 in 632.8 nm (Palik, 1985). Here it is important to point out that the wavelength values of 488.0 and 632.8 nm are known to be close to the plasmon excitation wavelength of Ag and Au, respectively. Increasing the metallic film thickness leads to decoupling of the top and bottom antenna.

For illustration purposes, Fig. 9 shows corresponding 2D numerical simulations carried out with Comsol Multiphysics® for TM-polarized waves for a 150 nm slit fabricated in an Ag film when illuminated by the line at 488.0 nm of an Ar ion laser. Fig. 9(a) shows the

amplitude of the magnetic H field (along the z direction). Figs. 9(b) and 9(c) shows the amplitude of the electric E field (in the y direction), with its vector representation in the x-y plane. Fig. 9(a) shows how the incident plane wave is modified by the existing subwavelength slit. It is possible to see that the considered wave is almost completely reflected from the unstructured part of the film. Around the slit entrance, the amplitude of the standing wave is markedly attenuated, where some lightwave transmission to the exit facet is apparent. On the dielectric/metal interface, a train of surface waves (SPPs) is evident together with waves propagating into space. In the rims, different charge configurations can be obtained, which can be symmetric or antisymmetrically coupled (Prodan et al., 2003). This coupling leads to determined charge configurations in each rim of the slit (top and bottom). From Figs. 9(b) and 9(c), these surface modes are clearly seen. It is possible to notice from the figures these resonances [antisymmetrically and symmetrically coupled in Figs. 9(b) and 9(c), respectively] on the facets of the slit. These modes are associated with localized SPs, which are nonpropagating excitations due to direct light illumination of the conduction electrons of the metallic nanostructure coupled to the electromagnetic field (Maier, 2007). A similar behaviour was observed in the simulations for Au films when

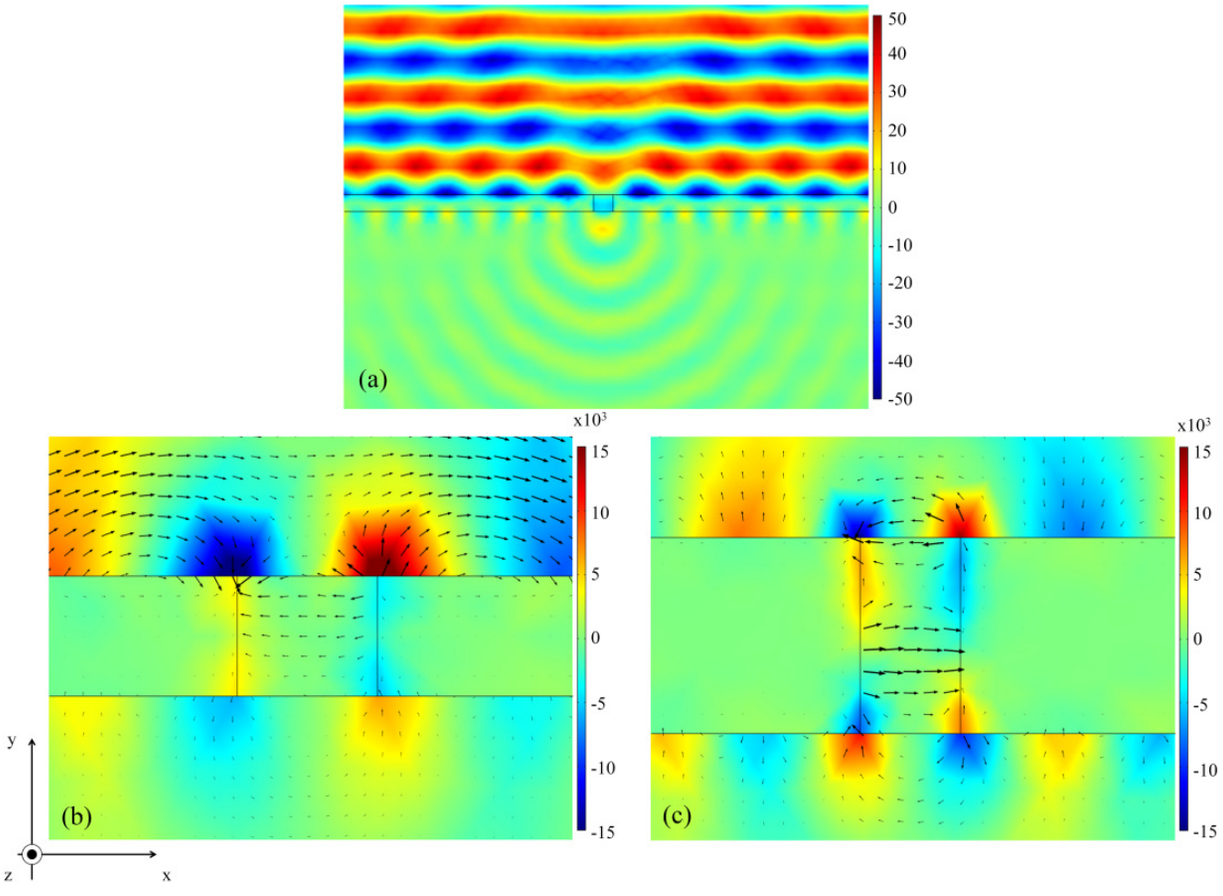

Figure 9. 2D numerical simulations of a 150 nm slit fabricated in an Ag film when illuminated by the line at 488.0 nm of an Ar ion laser. (a) Amplitude of the magnetic H field (along the z direction). (b) and (c) Amplitude of the electric E field (in the y direction), and its vector representation in the x-y plane. The value of the Ag film thickness in (a) and (b) is 120 nm, and in (c) is 270 nm. Length spans: (a) x = 4 μm and y = 2 μm, (b) and (c) x = 600 nm and y = 400 nm

excited by the line at 632.8 nm of an HeNe laser. The main apparent difference is the lower transmitted intensity due to a higher absorption loss attributable to the particular characteristics of Au (Palik, 1985), i.e., $\mathrm{Re}[\varepsilon_{Au}] = -9.49$ in contrast to $\mathrm{Re}[\varepsilon_{Ag}] = -7.89$. This is verified in Fig. 10, where it can be seen that the normalized transmission intensity for the Ag films is improved more than for the Au samples.

In general, the present numerical simulations qualitatively show appreciable light transmission through the slits. Actually, it was experimentally observed that the transmission sensitively depends on the metallic film thickness and slit width. As a first approximation, the theoretical slit transmission intensity can be given simply by the square modulus of Eq. (4). In this way, Fig. 10 plots as predicted [from Eq. (4)] and measured (using the setup shown in Fig. 7) transmission intensities as a function of the film thickness for the various slit widths milled in the Ag and Au samples. Also, the insets of Fig. 10 show the measured transmission versus slit width for certain film thicknesses. The relative slit transmission intensities are obtained by subtracting the background originating from the metal film and normalizing to the intensity from the wider slit structures. It is valuable to notice from Fig. 10 the very good correspondence between the theoretical estimate and the experiment. Therefore, taking into account the errors associated with the experimental determination of film thickness, slit width, and optical transmission intensities, it is possible to affirm that (1) the slits' transmission varies with metallic film thickness and presents a damped oscillatory behaviour as the film thickness increases, and (2) the transmission increases linearly with increasing slit width for a fixed metallic film thickness. Although the general behaviour is similar, distinct optical properties [see Fig. 4(a)] lead to perceptible differences in the transmitted intensity and the position of maxima and minima between the Ag and Au films.

To help in elucidating the first observation, it is valuable to note that Fabry–Perot (FP) resonances are expected to contribute to the enhanced transmission of subwavelength slit arrays (Porto et al., 1999; Takahura, 2001; Pang et al., 2007; Garcia-Vidal et al., 2002). In this way, FP modes related to the finite depth of the slits in the present films should give rise to transmission maxima at certain wavelengths (Garcia-Vidal et al., 2002). Actually, an accurate analysis recently published shows that the two maxima observed in Figs. 10(a) and 10(b) correspond to FP-like resonances within the slit volume for the first half-wave and full wave of the light within the slit (Weiner, 2011). In this sense, the FP multiple reflection effect within the slits leads to significant modulation of the transmission as a function of metal film thickness. These transmission maxima occur if the FP resonance condition is fulfilled (Li et al., 2009):

$$2k_0 \mathrm{Re}\left[\frac{\lambda_0}{\lambda_{SPP}}\right] t + \arg\left(\phi_1 \phi_2\right) = 2m_y \pi \tag{5}$$

where m_y (the FP mode) is an integer and ϕ_1 and ϕ_2 denote the phase of the reflection coefficients of the slit at the incident and output interfaces, respectively. Thus, the effect of slit depth on the transmission enhancement can be easily understood. When the incident wavelength and slit depth are satisfied by Eq. (5), a transmission maximum will occur. Furthermore, from Eq. (5), it is expected that the transmission under a certain incident wavelength has a period of $\lambda_{SPP}/2$ as a function of slit depth. The results of Fig. 10 can now

be simply explained for the present Ag and Au films. Therefore, when the film thickness is near half- or full-integer wavelengths of the guided mode within the slit "cavity", optimal transmission is achieved, which implies a field enhancement inside the slit.

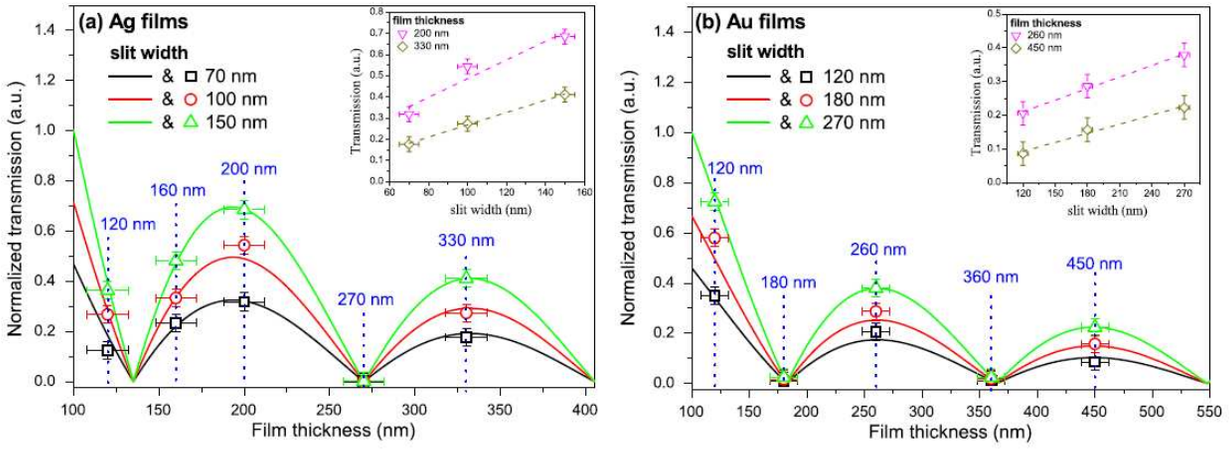

Figure 10. Theoretically estimated (lines) and experimental (symbols) normalized slit transmission intensities versus film thickness for the slits of the (a) 120, 160, 200, 270, and 330 nm thick Ag films, and the (b) 120, 180, 260, 360, and 450 nm thick Au samples. The dotted straight lines point out the thickness of the considered samples. The insets show the measured transmission versus slit width for some film thicknesses. Here, the dashed straight lines are linear fittings of the experimental points (Ferri et al., 2011)

We can apply an FP analysis to obtain the finesse F from Fig. 10, given by

$$F = \frac{\pi}{2\sin^{-1}\left(1/\sqrt{f}\right)} \tag{6}$$

where $f = 4R\left(1 - R\right)^{-2}$ is the finesse factor. Here, R is the reflectivity, given by R = 1 - T, where T is the transmission (Born et al., 1993). We determine from Fig. 10(a) for the Ag samples with 100 nm of slit width and thicknesses of 120, 160, 200, 270, and 330 nm, the reflectivities R = 0.73, 0.67, 0.46, 0.99, and 0.73, and the corresponding finesses F = 9.98, 7.74, 3.84, 312.58, and 9.89, respectively. From Fig. 10(b) for the Au samples with 120nm of slit width and thicknesses of 120, 180, 260, 360, and 450 nm, we determine the reflectivities R = 0.66, 0.99, 0.79, 0.98, and 0.91, and the resultant finesses F = 7.45, 312.58, 13.27, 155.49, and 33.29, respectively. Here it is important to point out that for an FP cavity, the definition of quality factor (Q factor) is equivalent to the finesse (Shyu et al., 2011). Therefore, we can clearly see that both the R and Q factor values are significantly affected by the film thickness for a fixed slit width. Also, it is interesting to notice that near-zero transmission is a sign of high reflectivity values and high Q factors. For the maximum transmission points, a backward reasoning applies.

Finally, the fact that the transmission increases linearly with increasing slit width is in accordance with literature (Kihm et al., 2008), where it was observed that the far-field

transmitted intensity from a single slit shows a monotonic increase with the width, as expected from macroscopic intuition. In other words, the physical cavity length L_z and the optical cavity length $L_c(\lambda)$ are related, such that $L_c(\lambda) = L_z + 2\delta(\lambda)\left|r(\lambda)\right|^2$, where $r(\lambda) = \left|r(\lambda)\right|\exp(i\phi)$ is the Fresnel coefficient, describes the shift of resonance wavelength from a perfect metal reflector due to field penetration $\delta(\lambda)$ into the metal mirror. But L_z is constant for all studied samples (20 μm), resulting in ϕ_z constant for a determined depth of metallic film. Nevertheless, the monotonic increase with the width w (= L_x) can also be explained considering FP resonances, for which we will use a simple analytical model to investigate the experimental results based on geometric arguments. Considering the standing wave mode in the cavity, when the penetration depth is ignored, the resonant condition of the slits can be written as

$$\frac{1}{\lambda_{SPP}^2} = \left(\frac{m_z + \phi_z}{2L_z}\right)^2 + \left(\frac{m_x + \phi_x}{2L_x}\right)^2 \tag{7}$$

We have applied Eq. (7) using the data of 200 nm of depth with widths L_x = 70, 100, and 150 nm for an Ag film, and 260 nm of depth with widths L_x = 120, 180, and 270 nm for an Au film. L_z = 20 μm for both samples. Also, we considered in our calculations that ϕ_z and ϕ_x are practically constant, since we did not observe any peak shift in the transmission spectra of the samples in analysis. In the interface, values of $\lambda_{SPP\text{-}Ag}$ = 269.9 nm and $\lambda_{SPP\text{-}Au}$ = 361.6 nm were used. It was obtained for the Ag film m_z = 78 and m_x = 1, 1.4, and 2, and for the Au film m_z = 145 and m_x = 1, 1.5, and 2, i.e., an increase in L_x allows an increase in the transmission intensity spectra for a fixed depth [see insets of Figs. 10(a) and 10(b)].

6.2. Multilayered metallic thin films

6.2.1. Motivation

Although the detailed picture of the transmission enhancement is still being investigated, the excitation of SPPs on the two surfaces of the metal film has been proposed to be involved in the process (Moreno et al., 2004; Lezec et al., 2004). In fact, it was already shown that when two perforated metal films are spaced by a dielectric layer (cascaded metallic structure), the transmission is further increased compared to a single perforated metal film (Ye et al., 2005). Additionally, bimetallic structures, such as films and nanoparticles, have attracted considerable attention for plasmon resonance excitation (Zynio et al., 2002; Gupta et al., 2005; Tan et al., 2007; Chen et al., 2010). These works are focused on improving sensitivity and evanescent field enhancement by optimization of the thickness of Ag/Au layers. Recently, optimization in terms of spectral characteristics was also theoretically demonstrated (Dyankov et al., 2011).

Here, we propose novel structures providing a unique opportunity to generate plasmonic modes. The structures are based on subwavelength slits fabricated in multilayered metallic thin films. The main feature of the novel structure is that the metal film consists of alternating layers of Ag and Au. In this Section, we demonstrate that the slits transmission can be augmented by increasing their widths, with the advantage to offer minor losses in comparison with a single perforated metal film.

6.2.2. Experimental considerations

The experimental procedure adopted here is similar to that shown in Section 6.1.2. Multilayered Ag/Au/Ag/Au and Au/Ag/Au/Ag films with total thickness t = 200 nm (d = 50 nm for each layer) were thermally evaporated onto BK7 glass substrates. Slits with widths in the range of approximately 60–600 nm were milled in the films using FIB lithography with the same already mentioned conditions. The slit length was fixed at 5 μm. For example, the right panel of Fig. 11 shows a scanning electron micrograph of a slit with width w about 180 nm fabricated in the Ag/Au/Ag/Au film.

The transmission measurement setup is identical to that shown in the left panel of Fig. 7. Here, the 488.0 nm wavelength light beam from the Ar ion laser was used for the Ag/Au/Ag/Au film, and the 632.8 nm wavelength light beam from the HeNe laser was used for the Au/Ag/Au/Ag sample. The left panel of Fig. 11 shows the basic schematic of the experimental setup.

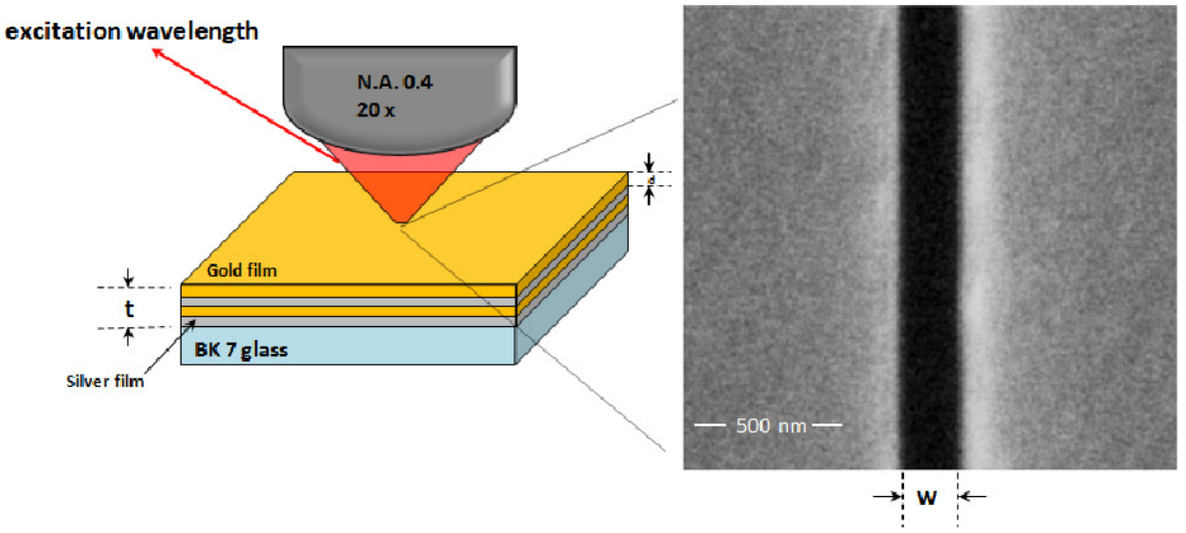

Figure 11. Left panel shows a simplified schematic of the optical transmission experiment. Similarly to the left panel of Fig. 7, a 488.0 nm (for the Ag/Au/Ag/Au film) and a 632.8 nm (for the Au/Ag/Au/Ag sample) Ar ion and HeNe laser light sources, respectively, are normally focused onto the sample surface by a 20× microscope objective lens. Right panel shows a scanning electron micrograph (taken with 60000× magnification) of a typical structure. The considered slit has approximately 180 nm of width and was focused-ion beam milled through the Ag/Au/Ag/Au sample. In the experiments, the total thickness t of the Ag/Au/Ag/Au and Au/Ag/Au/Ag films was fixed at 200 nm. The width w is varied from 60 nm to 600 nm (Ferri et al., 2012)

6.2.3. Results and discussion

Fig. 12(a) shows the physical picture adopted in this work to investigate the light transmission through the subwavelength slits fabricated in the multilayered metallic films. The essential elements of the model are represented (Gay et al., 2006b). Basically, an incident monochromatic light beam in air is linearly polarized perpendicular to the slit of subwavelength width w, milled in a multilayered metallic film with thickness t, deposited on a dielectric substrate (BK7 glass). Each metallic layer has a thickness d (= 50 nm).

The physical processes involved in the far-field intensity enhancement for the present subwavelength slits are similar to those discussed in Section 6.1.3, in the sense that the first metallic layer is responsible to start the generation of plasmonic excitations. Form our simulation results we can see that at the interface between the adjacent metallic layers the condition for generation of SPPs is not fulfilled, Fig. 12(b). Nevertheless, there is an induced charge current due to the plasmonic surface excitations from the first to the last metallic layer, see Fig. 12(c), resulting in an asymmetric distribution [similar to Fig. 9(b)]. Additionally, the transmission over each layer is given by the Beer-Lambert law, i.e., $I_i = I_{i-1}\exp(-\alpha d)$ (Born et al., 1993), where α is the absorption coefficient of the corresponding metal layer, d is the thickness of the layers, and i is the layer number. Then, the resulting transmitted intensity can be written as (Gay et al., 2006b; Maier, 2007; Pacifici et al., 2008; Ferri et al., 2011),

$$I_{out} = I_i + \left| \frac{E_0}{\pi} \frac{w}{t} \cos\left(k_{SPP} t + \frac{\pi}{2} \right) \right|^2 , \; i = 1,...,4 \tag{8}$$

Here, the physical quantities of the second term are identical with those in Eq. (4). The only difference is that the considered dielectric medium is the air, which tabulated dielectric constant is $\varepsilon_{air} = 1.00$ (Palik, 1985). In this sense, the first layer is assumed to govern the extraordinary transmission (I_{SPP}) of the subwavelength slits fabricated in the present multilayered metallic films.

Numerical simulations carried out with Comsol Multiphysics® were also performed for the multilayered metallic samples. A similar behaviour was observed in comparison to that shown in Section 6.1.3. For illustration purposes, Figs. 12(b) and 12(c) show simulations for a 50 nm slit fabricated in the Au/Ag/Au/Ag film when illuminated by the line at 632.8 nm typical of an HeNe laser. Fig. 12(b) shows the amplitude of the magnetic H field (along the z direction). Fig. 12(c) shows the amplitude of the electric E field (in the y direction), with its vector representation in the x-y plane.

The theoretical slit transmission intensity can be given by Eq. (8). In this way, Fig. 13 plots as predicted and measured transmission intensities as a function of the slit width for the various subwavelength structures milled in the Ag/Au/Ag/Au and Au/Ag/Au/Ag samples. For comparison purposes, the insets of Fig. 13 also show the simulated slit optical transmission obtained from Comsol Multiphysics® versus slit width for the considered multilayered metallic films and single perforated Ag and Au films with 200 nm of thickness. The relative slit transmission intensities are obtained by subtracting the background originating from the metal film and normalizing to the intensity from the wider slit structures. It is valuable to notice from Fig. 13 the very good correspondence between the theoretical estimative and experiment. Therefore, it is possible to affirm that: (1) the transmission increases linearly with increasing slit width, and (2) for a fixed width, the transmission of the multilayered structures is augmented in comparison with a single perforated metal film of the same thickness. It is evident that this last observation is more apparent for the Au/Ag/Au/Ag film.

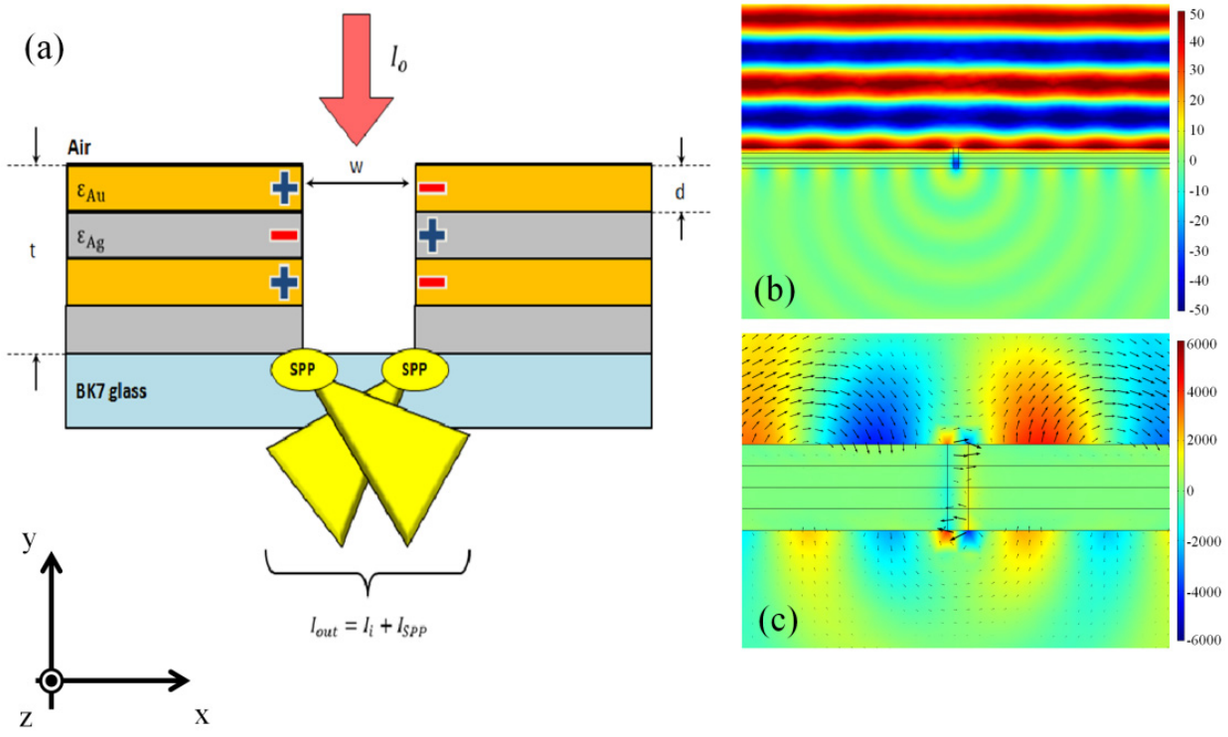

Figure 12. (a) Illustration of the adopted model. A single frequency incoming plane wave with intensity I_0 in air is linearly polarized perpendicular to a slit of subwavelength width w, milled in a multilayered metallic film with thickness t deposited on a BK7 glass substrate. Each metallic layer has a thickness d. The overall transmitted intensity I_{out} is a sum of the transmission of each layer I_i with the contribution due to the SPPs created in the air/metallic film interface I_{SPP}. (b) and (c) 2D simulations of a slit fabricated in the Au/Ag/Au/Ag film. (b) Amplitude of the magnetic H field (along the z direction). (c) Amplitude of the electric E field (in the y direction), and its vector representation in the x-y plane. Length spans: (b) x = 4 μm and y = 2 μm, and (c) x = 600 nm and y = 400 nm (adapted from Ferri et al., 2012)

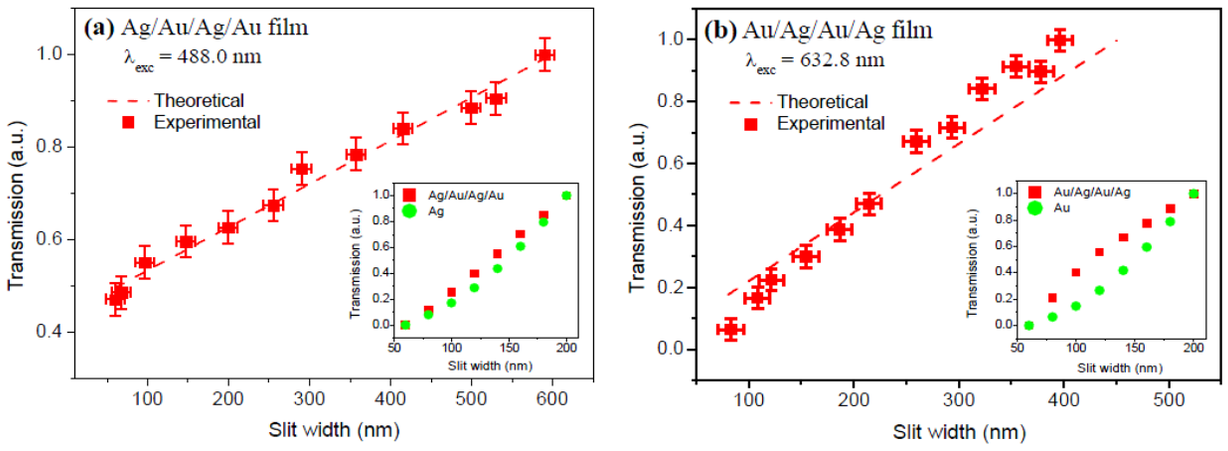

Figure 13. Theoretically estimated (dashed straight lines) and experimentally obtained (squares) normalized slit transmission intensities versus slit width for the various subwavelength structures milled in the (a) Ag/Au/Ag/Au and (b) Au/Ag/Au/Ag samples. The insets show details of the simulated slit optical transmission versus slit width for the considered metallic multilayered films and single perforated Ag and Au films with 200 nm of thickness (Ferri et al., 2012)

The fact that the far-field transmitted intensity from the present slits shows a monotonic increase with their widths is in the same trend of that previously observed in single perforated metal films (Ferri et al., 2011; Kihm et al., 2008), as expected from macroscopic intuition. In that case, the dependence could be explained considering Fabry-Perot resonances of the standing wave mode in the slit "cavity", in conjunction with the generation of SPPs. However, in the present case, such a resonant condition (Ferri et al., 2011; Kihm et al., 2008; Li et al., 2009) cannot be applied, since we have distinct reflection coefficients due to the existence of different materials in the slits. Nevertheless, the monotonic increase with the width is expected simply by considering the dependence of the transmitted intensity with the w parameter in Eq. (8).

Finally, the observation that the transmission of the metallic multilayered structures is augmented in comparison with a metal film of the same thickness when perforated with subwavelength slits, can be elucidated considering that, for the present multilayered films, the optical transmission profile is assumed to be mainly governed by the first metallic layer,

given that it is responsible to start the generation of plasmonic excitations. Subsequently, we just have electronic conduction to the underlying metallic layers, as already pointed out. Furthermore, each metallic layer (with 50 nm of thickness) additionally contribute to the overall transmission according to the Beer-Lambert law, in contrast to a single perforated metal film with the same total thickness of 200 nm of the proposed multilayered films.

Independently of the preceding discussion about multilayered metallic thin films, it is valuable to mention that gain-assisted propagation of SPPs at the interface between a metal and a dielectric with optical gain have been the focus of much research activity (Avrutsky, 2004; Nezhad et al., 2004). In this context, Er^{3+}-doped tellurite glasses as the dielectric medium is very attractive (Wang et al., 1994). Very recently, our research group have gave significant contributions regarding the excitation and/or improvement of the luminescence of Er^{3+} ions embedded in these glassy matrices through plasmonic nanostructures (Rivera et al., 2012a; Rivera et al., 2012b).

7. Conclusion

The physics of the transmission of light through subwavelength apertures in metallic films has been a topic of intense research in recent times. In this chapter, we have presented a review of this field, showing some essential subjects involved in this phenomenon. Although the current understanding of this phenomenon is not complete or even not substantially correct, the materials presented in many literatures are useful and clue us on how to go ahead. In particular, we presented in this chapter some contributions of our research group regarding the optical transmission through subwavelength single slits in metallic thin films. The simulations qualitatively reveal that the transmission profile is controlled by interference between the incident standing wave and plasmonic surface excitations. It was possible to observe that the slits' transmission is significantly affected by the metallic film thickness, presenting a damped oscillatory behavior as the film thickness is augmented. In addition, for a fixed metallic film thickness, the transmission increases linearly with increasing slit width. For a fixed wavelength and slit width, FP modes within

the slits lead to significant modulation of the transmission as a function of metal film thickness. As well, it was shown that the transmission of multilayered structures is augmented in comparison with a single perforated metal film with a similar thickness. In this sense, we have demonstrated that metallic multilayered structures have the advantage to offer minor losses in comparison with a single perforated metal film.

Author details

V. A. G. Rivera, F. A. Ferri, O. B. Silva, F. W. A. Sobreira and E. Marega Jr.
Instituto de Física de São Carlos, Universidade de São Paulo, São Carlos, Brazil

Acknowledgement

The authors are indebted to Prof. J. Weiner, Prof. A. R. Zanatta and Dr. M. A. Pereira-da-Silva (all at the Instituto de Física de São Carlos, USP, Brazil) for the helpful discussions, optical transmission experiments and atomic force microscopy measurements, respectively. We also would like to thanks Prof. B.-H. V. Borges (Departamento de Engenharia Elétrica, EESC, USP, Brazil) for the support with Comsol Multiphysics®. This work was financially supported by the Brazilian agencies FAPESP and CNPq under CEPOF/INOF.

8. References

Avrutsky, I. (2004). Surface Plasmons at Nanoscale Relief Gratings between a Metal and a Dielectric medium with Optical Gain. *Physical Review B*, Vol.70, No.15, pp. 155416-1 – 155416-6

Bethe, H.A. (1944). Theory of diffraction by small holes. *Physical Review*, Vol.66, No.7–8, (October), pp. 163–182.

Born, M. & Wolf, E. (1993). Principles of Optics: Electromagnetic Theory of Propagation Interference and Diffraction of Light (Pergamon), ISBN 978-008-0139-87-6, Cambridge, United Kingdom.

Bouhelier, A., Huser, T., Tamaru, T. et al. (2001). Plasmon optics of structured silver films. *Physical Review B*, Vol. 63, No. 15, (March) pp. 155404-1 – 155404-9.

Bouwkamp, C.J. (1950). On Bethe's Theory of Diffraction by Small Holes. *Philips Research Reports*, Vol.5, No.5, pp. 321–332.

Bouwkamp, C.J. (1950). On the Diffraction of Electromagnetic Waves by Small Circular Disks and Holes. *Philips Research Reports*, Vol.5, No.6, pp. 401–422.

Bouwkamp, C.J. (1954). Diffraction theory. *Reports on Progress in Physics*, Vol.17, No.1 pp. 35–100.

Chen, X. & Jiang, K. (2010). Effect of aging on optical properties of bimetallic sensor chips. *Optics Express*, Vol.18, No.2, pp.1105-1112.

Degiron, A., et al.(2004). Optical Transmission Properties of a Single Subwavelength Aperture in a Real Metal. *Optics Communications*, Vol.239, No.1-3, pp.61–66.

Ditlbacher, H., et al. (2002). Fluorescence Imaging of Surface Plasmon Fields. *Applied Physics Letters*, Vol.80, No.3, pp. 404–406.

Ditlbacher, H., et al.(2002). Two-dimensional Optics with Surface Plasmon Polaritons. *Applied Physics Letters*, Vol.81, No.10, pp. 1762–1764.

Dyankov, G., et al.(2011). Plasmon Modes Management. *Plasmonics*, Vol.6, No.4, pp. 643–650

Ebbesen, T.W., et al. (1998). Extraordinary optical transmission through sub-wavelength hole arrays. *Nature*, Vol.391, pp. 667–669.

Ferri, F.A., et al. (2011). Influence of Film Thickness on the Optical Transmission Through Subwavelength Single Slits in Metallic Thin Films. *Applied Optics*, Vol.50, No.31, pp. G11-G16.

Ferri, F.A. et al. (2012). Surface Plasmon Propagation in Novel Multilayered Metallic Thin Films. *Proceedings of SPIE*, Vol.8269, pp. 826923-1-826923-6, San Francisco, USA, January 23-26, 2012.

Fontana, E. (2006). Thickness Optimization of Metal Films for the Development of Surface-Plasmon-based Sensors for Nonabsorbing Media. *Applied Optics*, Vol.45, No.29, pp.7632–7642.

Forbes, R. & Djuric, Z (1996). Progress in understanding liquid-metal ion source operation *9th International Vacuum Microelectronics Conference*, pp.468-472, Saint Petersburg, Russia, July 7-12, 1996.

Garcia-Vidal, F.J. & Martin-Moreno, L. (2002). Transmission and Focusing of Light in One-Dimensional Periodically Nanostructured Metals. *Physical Review B*, Vol.66, No.15, pp. 155412-1 – 155412-10.

Garcia-Vidal, F.J. et al.(2010). Light Passing Through Subwavelength Apertures, *Reviews of Modern Physics*, Vol.82, No.1, pp. 729-787.

Gay, G. et al.(2006). Surface Wave Generation and Propagation on Metallic Subwavelength Structures Measured by Far-field Interferometry. *Physical Review Letters*, Vol.96, No.21, pp. 213901-1 – 213901-4.

Gay, G. et al.(2006). The Optical Response of Nanostructured Surfaces and the Composite Diffracted Evanescent Wave Model. *Nature Physics*, Vol.2, No.4, pp. 262–267.

Ghaemi, H.F., et al.(1998). Surface Plasmons Enhance Optical Transmission through Subwavelength Holes. *Physical Review B*, Vol.58, No.11, pp. 6779–6782.

Gupta, B.D. & Sharma, A.K.(2005). Sensitivity Evaluation of a Multi-layered Surface Plasmon Resonance-based Fiber Optic Sensor: a Theoretical Study. *Sensors and Actuators B:Chemical* Vol.107, No.1, pp. 40-46.

Hecht, B., et al.(1996). Local Excitation, Scattering, and Interference of Surface Plasmons. *Physical Review Letters*, Vol. 77, No. 9, pp. 1889–1892.

Huang, C.P., et al.(2007). Plasmonics:Manipulating Light at the Subwavelength Scale. *Active and Passive Electronic Components*, Vol.2007, No.30946, pp.1-13.

Hutter, E. & Fendler, J.H.(2004). Exploitation of Localized Surface Plasmon Resonance. *Advanced Materials*, Vol. 16, No. 19, pp. 1685–1706.

Jackson, J.D. (1999). Classical Electrodynamics. (John Wiley & Sons, Inc., New York, NY, 3rd edition), ISBN 978-047-1309-32-1.

Janssen, O.T.A., et al.(2006). On the Phase of Plasmons Excited by Slits in a Metal Film. *Optics Express*, Vol.14, No.24, pp.11823–11832.

Kalkum, F., et al.(2007). Surface-wave Interferometry on Single Subwavelength Slit-groove Structures Fabricated on Gold Films. *Optics Express*, Vol.15, No.5, pp. 2613–2621.

Kihm, H.W., et al.(2008). Control of Surface Plasmon Generation Efficiency by Slit-width Tuning. *Applied Physics Letters*, Vol.92, No.5, pp.051115-1 – 051115-3.

Kim, J.H. & Moyer, P.J.(2006). Thickness Effects on the Optical Transmission Characteristics of Small Hole Arrays on Thin Gold Films. *Optics Express*, Vol.14, No.15, pp.6595–6603.

Lalanne, P., et al.(2005). Theory of Surface Plasmon Generation at Nanoslit Apertures. *Physical Review Letters*, Vol.95, No.26, pp. 263902-1 – 263902-4.

Lal, S., et al.(2007). Nano-optics from Sensing to Waveguiding. *Nature Photonics*, Vol.1, No.11, pp. 641-648.

Laluet, J.-Y., et al.(2008). Generation of Surface Plasmons at Single Subwavelength Slits: from Slit to Ridge Plasmon. *New Journal of Physics*, Vol.10, No.10, pp. 105014-1 – 105401-9.

Langford R, et al.(2007). Focused Ion Beam Micro- and Nanoengineering. *MRS Bulletin*, Vol.32, No.5, pp. 417–423.

Lezec, H.J. & Thio, T.(2004). Diffracted Evanescent Wave Model for Enhanced and Suppressed Optical Transmission through Subwavelength Hole Arrays. *Optics Express*, Vol.12, No.16, pp. 3629–3651.

Li, Z.-B, et al.(2009). Fabry–Perot Resonance in Slit and Grooves to Enhance the Transmission through a Single Subwavelength Slit. *Journal of Optics A: Pure and Applied Optics*, Vol.11, No.10, pp. 1-4.

Lindquist, N.C. et al.(2012). Engineering Metallic Nanostructures for Plasmonics and Nanophotonics. *Reports on Progress in Physics*, Vol.75, No.3, pp. 1-61.

Maier, S. A. (2007). Plasmonics: Fundamentals and Applications. (Springer). ISBN 978-0387-33150-8.

Melngailis, J. (1987). Focused Ion Beam Technology and Applications. *Journal of Vacuum Science and Technology B: Microelectronics and Nanometers Structures*, Vol.5, No.2, pp.469-495.

MoberlyChan, W., et al.(2007). Fundamentals of Focused Ion Beam Nanostructural Processing: Below, at, and Above the Surface. *MRS Bulletin*, Vol.32, No.5, pp. 424–432.

Moreno, L. M. & Garcia-Vidal, F. J. (2004). Optical Transmission through Circular Hole arrays in Optically Thick Metal Films. *Optics Express*, Vol.12(16), No.16, pp. 3619-3628.

Nezhad, M., et al.(2004). Gain Assisted Propagation of Surface Plasmon Polaritons on Planar Metallic Waveguides. *Optics Express*, Vol.12, No.17, pp. 4072-4079.

Orloff, J. (1993). High-Resolution Focused Ion Beams. *Review of Scientific Instruments*, Vol.64, No.5, pp. 1-26.

Pacifici, D., et al.(2008). Quantitative Determination of Optical Transmission through Subwavelength Slit Arrays in Ag films: Role of Surface Wave Interference and Local Coupling between adjacent Slits. *Physical Review B*, Vol.77, No.11, pp. 1-5.

Palik, E.D.(1985). Handbook of Optical Constants of Solids. (Academic Press). ISBN 0125444206

Pang, Y., et al.(2007). Optical Transmission through Subwavelength Slit Apertures in Metallic Films. *Optics Communications*, Vol.280, No.1 pp. 10–15.

Porto, J.A., et al.(1999). Transmission Resonances on Metallic Gratings with very Narrow Slits. *Physical Review Letters*, Vol.83, No.14, pp. 2845–2848.

Prodan, E, et al.(2003). A Hybridization Model for the Plasmon Response of Complex Nanostructures. *Science*, Vol.302, No.5644, pp. 419–422.

Reyntjens, S. & Puers, R.(2001). A Review of Focused Ion Beam Applications in Microsystem Technology. *Journal of Micromechanics and Microengineering*, Vol.11, No.4, pp.287-300.

Rivera, V.A.G., et al.(2012). Focusing Surface Plasmons on Er 3+ Ions with Convex/Concave Plasmonic lenses. *Proceedings of SPIE*, Vol.8269, pp.82692I-1 – 8269I-6, San Francisco, USA, January 23-26, 2012.

Rivera, V.A.G., et al.(2012). Luminescence enhancement of Er 3+ Ions from Electric Multipole Nanostructure Arrays. *Proceedings of SPIE*, Vol.8269, pp.82692H-1 – 8269H-7, San Francisco, USA, January 23-26, 2012.

Sarid, D.(1981). Long-range Surface-plasma waves on very thin metal films. *Physical Review Letters*, Vol. 47, No. 26, pp. 1927–1930.

Shou, X., et al.(2005). Role of Metal Film Thickness on the Enhanced Transmission Properties of a Periodic Array of Subwavelength Apertures. *Optics Express,* Vol.13, No.24, pp.9834–9840.

Shyu, L.-H., et al.(2011). Influence of Intensity loss in the Cavity of a Folded Fabry–Perot Interferometer on Interferometric Signals. *Review of Scientific Instruments*, Vol.82, No.6, pp. 063103-1 – 063103-3.

Takakura, Y.(2001). Optical Resonance in a Narrow Slit in a Thick Metallic Screen. *Physical Review Letters*, Vol.86, No.24, pp. 5601–5603.

Tan, Y.Y., et al.(2007). Two-layered Metallic Film Induced Surface Plasmons for Enhanced Optical Propulsion of Microparticles. *Applied Physics Letters*. Vol.91, No.14, pp.141108-1-141108-3.

Tao T, et al.(1990). Focused ion beam Induced Deposition of Platinum. *Journal of Vacuum Science and Technology B: Microelectronics and nanometer structures*. Vol.8, No.6, pp.1826-1829.

Treacy, M.M.J.,(1999). Dynamical Diffraction in Metallic Optical Gratings. *Applied Physics Letters*, Vol.75, No.5, pp. 606–608.

Treacy, M.M.J.,(2002) Dynamical Diffraction Explanation of the Anomalous Transmission of Light through metallic gratings. *Physical Review B*, Vol.66, No.19. pp.195105-1–191505-11.

Volkert, C.A. & Minor, A.M.(2007). Focused Ion Beam Microscopy and Micromachining. *MRS Bulleting*, Vol.32, No.5, pp. 389-395.

Wang, J.S., et al.(1994). Tellurite glass: a new candidate for fiber devices. *Optical Materials*, Vol.3, No.3, pp.187-203

Weiner, J.(2009). The Physics of Light Transmission through Subwavelength Apertures and Aperture Arrays. *Reports on Progress in Physics*, Vol.72, No.6, pp. 1-19.

Weiner, J.(2011). The Electromagnetics of Light Transmission through Subwavelength Slits in Metallic Films. *Optics Express*, Vol.19, No.17, pp. 16139–16153.

Xie, Y., et al.(2005). Transmission of Light through a Periodic Array of Slits in a Thick Metallic Film. *Optics Express*, Vol.13, No.12, pp.4485–4491.

Ye, Y.H. & Zhang, J.Y.(2005). Enhanced Light Transmission through Cascaded Metal Films Perforated with Periodic Hole Arrays. *Optics Letters*, Vol.30, No.12, pp.1521-1523.

Yin, L., et al.(2004). Surface Plasmons at single nanoholes in Au films. *Applied Physics Letters*, Vol.85, No.3, pp. 467–469.

Zayats, A.V., et al.(2005). Nano-optics of Surface Plasmon Polaritons. *Physics Reports*, Vol.408, No.3-4, pp. 131–314.

Zynio, S.A., et al.(2002). Bimetallic layers increase sensitivity of affinity sensors based on surface plasmon resonance. *Sensors*, Vol.2, No.2, pp. 62-70.